# Research On the Leakage Identification Method of the Hydrogen Doping Station Site Based On Image Processing

**Yao Liu[a], Haiyang Yu[a], Xiaopeng Yu[a], Qingqing Xu[a*], Laibin Zhang[a], Yuanliang Jiang[b], Haipeng Liu[b]**

[a]College of Safety and Ocean Engineering, China University of Petroleum (Beijing), Beijing, China
[b]Research Institute of Petroleum Exploration & Development, PetroChina, Beijing , China

**Abstract:** Utilizing the existing natural gas pipeline network for hydrogen transportation is a primary approach in the field. However, introducing hydrogen into natural gas alters the operational conditions of pipelines and equipment, leading to a reduction in the lower limit of natural gas explosion and an increase in leakage diffusion rate. Consequently, this poses more severe risks of gas leakage and explosions. Conventional detection methods solely provide numerical values representing gas concentration, lacking intuitive judgment capability.This paper employs an infrared gas imaging leakage detection method to visualize leaking gas and designs an intelligent detection algorithm for hydrogen-blended natural gas leaks based on image processing. To obtain more infrared gas imaging data, a hydrogen-blended natural gas leakage experimental platform was constructed, and experimental validation was conducted. The results show that after training the model on a self-constructed hydrogen-blended natural gas leakage imaging dataset, the detection accuracy reached 98%, providing a viable solution for gas leakage detection.

**Keywords:** Mixed with hydrogen gas,Infrared imaging of gas,object detection,Gas leakage detection

## 1. INTRODUCTION

The use of pipelines for hydrogen transportation, due to its advantages of long-distance, economical, and large-scale, is becoming an inevitable choice to promote the development of hydrogen energy storage and transportation. Hydrogen blending with natural gas utilizes existing infrastructure to enable cost-effective and large-scale hydrogen transport, but it also increases the risk of gas leakage. After hydrogen is blended, the gas leakage rate increases, and its density decreases, thereby increasing the diffusion efficiency of the gas in the air[1]. Furthermore, hydrogen-blended natural gas has a lower explosion limit, significantly increasing the explosion risk. Therefore, effective gas leakage detection is crucial for preventing explosive accidents and reducing the damage caused by such accidents.

Optical gas imaging (OGI) infrared thermography can capture environmental temperature changes caused by gas leakage to detect leakage points and display the leakage situation through images[2]. Non-contact gas leakage detection technology based on infrared imaging can achieve quick response and long-distance monitoring, covering a wide range and providing intuitive results. However, currently, it is limited to displaying images of gas leaks, and the occurrence of leaks still relies on subjective judgment by personnel, failing to achieve automated detection[3]. Subjective judgment depends on the level and experience of the inspection personnel, leading to high labor costs and varying judgment results under the same conditions, lacking standardized evaluation[4].

With the advancement of technology, many researchers have combined optical gas imaging with artificial intelligence to achieve intelligent gas leak detection[5-8]. This integration has reduced labor costs and made pipeline transportation safer and more efficient. Techniques such as Faster R-CNN[9] and SSD[10] are prominent examples. Faster R-CNN offers higher accuracy but is computationally more complex and time-consuming. SSD, while better suited for small object detection and offering a good balance between accuracy and computation speed, still struggles to achieve real-time detection. Therefore, infrared imaging detection of hydrogen-blended natural gas leaks faces the following challenges:

a) lack of high-quality datasets for model training.
b) Improving detection speed to achieve real-time performance while maintaining accuracy.

## 2. LEAKAGE EXPERIMENT

To address the above issues, this paper proposes an intelligent detection algorithm for hydrogen-blended natural gas leakage based on object detection algorithms. The algorithm improves the accuracy of detection by addressing the issues of low resolution, grayscale images, and blurry edge contours in infrared gas images. To obtain more infrared gas imaging data, an experimental platform for simulating hydrogen-blended natural gas leakage was constructed in proportion, and experimental verification was conducted. The flowchart is shown in Figure 1, with the steps as follows:

a) Construct an experimental platform for hydrogen-blended natural gas leakage, simulate leakage detection under different conditions, and obtain infrared images of hydrogen-blended natural gas leakage.

b) Based on the infrared imaging characteristics of hydrogen-blended natural gas leakage, outline and label the location of the leaking gas during the image preprocessing stage.

c) During the model training stage, train the data of hydrogen-blended natural gas leakage images and optimize the model using the YOLOv5 convolutional neural network algorithm.

d) Evaluate the real-time leakage detection model of hydrogen-blended natural gas.

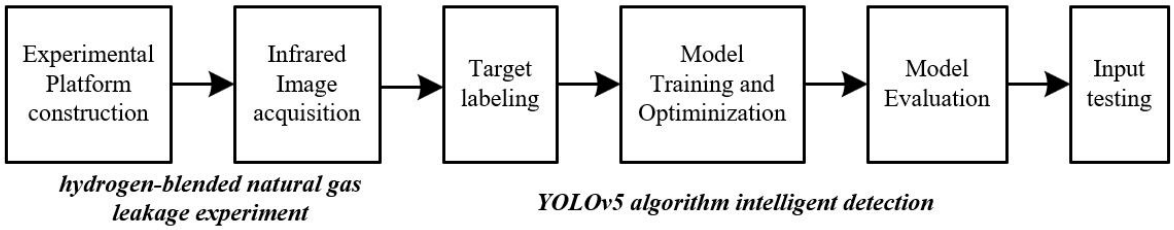


Figure 1. Hydrogen-blended Natural Gas Leak Recognition Detection Process

This experiment employs infrared thermography detection technology to detect hydrogen-blended natural gas leakage. The basic principle of gas infrared thermography is based on the infrared absorption spectrum characteristics of the gas, relying on temperature differences to distinguish between the leaking gas and the background. The thermal imager detects the infrared wavelength band that includes a specific absorption peak of the gas, displaying the leaking gas image in grayscale to show radiation changes that are invisible to the human eye. Research has found that the factors affecting the detection results of gas infrared thermal imagers are mainly as follows: (1) Temperature difference between the gas and the background. When the background temperature is higher than the leaking gas temperature, the gas appears dark in the image, and vice versa, it appears bright. The imaging effect is influenced by the temperature difference between the two. (2) Imaging distance. Detection distance is the most important parameter affecting detection accuracy. As the detection distance increases, atmospheric radiation loss also increases, thereby reducing the radiation difference between the gas and the background, affecting the imaging effect. (3) Gas concentration. The distribution of gas concentration in space is uneven. According to the Beer-Lambert law, gas concentration and gas path length affect the spectral transmittance. When the concentration is higher and the path length is longer, the gas absorbs more background radiation, making the imaging effect more apparent.

Based on these factors, a hydrogen-blended natural gas leakage experiment can be designed by setting experimental variables according to the factors affecting gas infrared thermal imaging. This approach enriches the dataset samples for subsequent model training. The experiment is conducted at the Hydrogen Energy Experimental Base in Shandong Province, China, where a hydrogen-blended natural gas pipeline leakage experimental area is set up as shown in Figure 2. This area can introduce pre-mixed gases with different hydrogen blending ratios, with a pipe diameter of 40mm and different orifice sizes to simulate leakage. The gas infrared imaging equipment used is the GL1000i refrigerated gas leak detector produced by Ke Yi Optoelectronics, capable of clearly observing gas leakage under different environments. It is primarily designed for the oil and petrochemical industry to detect gas leaks. Equipped with a cooled detector with a resolution of $320 \times 256$ and a high sensitivity of up to 15mK, it can clearly observe gas leaks under various environmental conditions. Relevant parameters are shown in Table 1.


Figure 2. Hydrogen-blended Natural Gas Pipeline Leakage Pilot Area

Table 1. Relevant Parameters of the Infrared Leakage Detector

| content | Technical Indicators |
|---|---|
| Types of detectors | Refrigeration detector |
| Infrared resolution | 320×256 |
| sensitivity | 15mk |
| Work band | 3.2~3.5μm |
| Temperature measurement range | -20℃~+350℃ |
| Digital zoom | 1-16x continuous zoom |

Data is collected under two conditions: direct sunlight at noon and low nighttime temperatures without external light sources. Three different imaging distances are set: 2m, 5m, and 8m. The gas leakage rate is adjusted by changing the inlet pressure and orifice size. Experiments are conducted with hydrogen blending ratios of 5%, 10%, and 15%. The overall experimental variables and parameters are shown in Table 2.

Table 2. Experimental Variants and Parameters

| variant | parameters | | |
|---|---|---|---|
| Lighting (shooting time) | 10：00~14：00 | 21：00~23：00 | |
| Whether the lens is moving | Handheld device forward shot | Fixed-camera shooting | |
| Shooting Distance | 2m | 5m | 8m |
| hydrogen blending ratio | 5% | 10% | 15% |
| leakage rate | 3~5SLM | 5~7SLM | 7~10SLM |

To include all different variables, there should be 108 sets of conditions, with each condition being filmed twice, and a fixed filming time of 20 seconds. Since the gas plume may be unstable at the beginning and end of the video, the first 5 seconds and the last 5 seconds of the video are excluded, capturing only the middle 10 seconds to obtain stable gas leakage images. Ultimately, a dataset containing 216 videos is obtained (with a frame rate of approximately 15 frames per second, recording a total of about 32,400 frames). The collected infrared imaging pictures of hydrogen-blended natural gas leakage are labeled using Labelimg, resulting in a complete dataset.

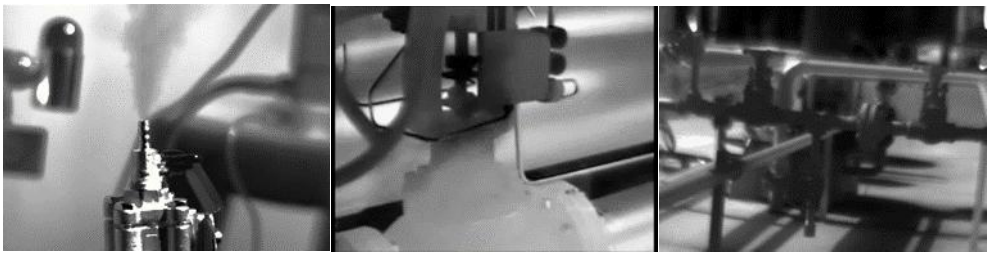

Figure 3. Hydrogen-blended Natural Gas Leakage Images

## 3. INTELLIGENT ALGORITHM DETECTION TECHNOLOGY

Deep learning-based object detection algorithms primarily focus on two directions: two-stage algorithms such as the R-CNN series and one-stage algorithms such as YOLO and SSD. One-stage algorithms directly predict the class probabilities and position coordinates of objects without the refinement step, making this method faster in detection. The YOLO series of algorithms innovatively integrate classification, localization, and detection into a single network, making it faster to operate and avoiding the misjudgment of background as targets, thereby reducing false detection rates. Due to its fast detection speed, YOLO is often used in fields such as video and surveillance for real-time detection. In this paper, due to the requirement for quick response time in gas leakage detection, the YOLO algorithm is selected for object detection to achieve real-time detection.

### 3.1. Network Model Construction

As an open-source code, YOLOv5 has been continuously improved, making it easier to use, train, and deploy. Therefore, this paper selects YOLOv5 for hydrogen-blended natural gas leakage detection. Its network structure is shown in Figure 4 and is mainly divided into three parts: the backbone, the neck, and the head. The input image size for the model is 3×640×640, and in the head part, it can output images in three sizes (255×80×80, 255×40×40, 255×20×20). The other network modules are introduced as follows:

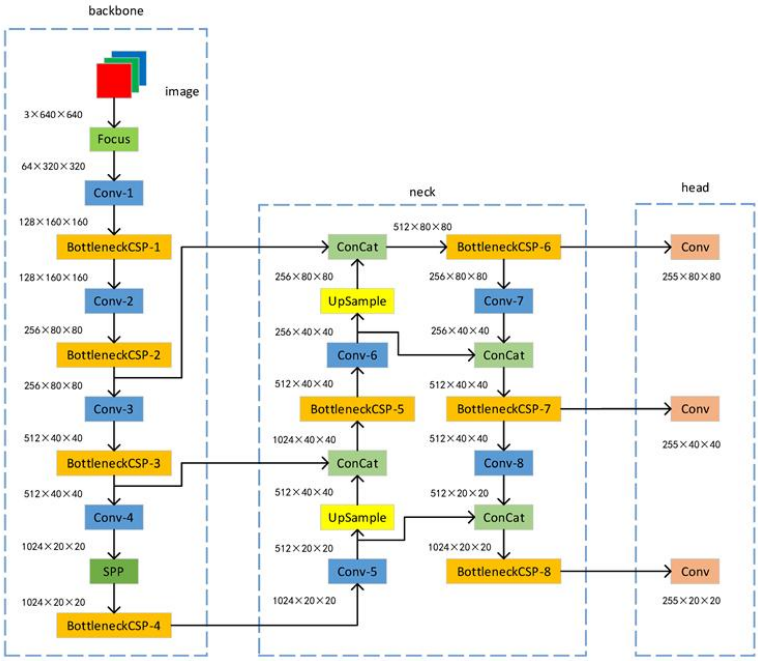


Figure 4. YOLOv5 Model Network Structure

a) Backbone

The Focus module performs initial processing on the input image, focusing on different parts of the image to improve the effect of subsequent processing. Conv-1 to Conv-4 are all convolutional layers used to extract low-level features of the image. BottleneckCSP-1 to BottleneckCSP-4 are connected after the corresponding convolutional layers, used to build deep residual learning for the model, maintaining network depth and performance while reducing computational complexity. After Conv-4, there is an SPP module, which is a spatial pyramid pooling layer that can extract features of different sizes, enhancing the model's ability to adapt to targets of various sizes.

b) Neck

The Conv-5 to Conv-8 convolutional layer modules further process the features, increasing their depth and complexity. The UpSample layer, a top-down approach, enlarges the feature map size, allowing the low-resolution deep-layer feature maps to match the large-size shallow-layer feature maps. The Contact feature concatenation module is also used to enhance the feature representation capability.

c) Head

Finally, the convolutional layers output the final detection results, including the position of the bounding boxes, the class of the objects, and the confidence scores.

### 3.2. Model Training

The official YOLOv5 code provides five versions: YOLOv5n, YOLOv5s, YOLOv5m, YOLOv5l, and YOLOv5x. Based on the performance test diagrams of these models pre-trained on the COCO dataset, comprehensive analysis shows that YOLOv5s achieves higher AP indicators while maintaining a relatively fast inference speed. Therefore, this study selects the YOLOv5s model for dataset training. Through transfer learning, the trained model parameters are transferred to the new model to assist in training, so that the model training does not start from scratch, thereby shortening the training time to a certain extent. This paper uses the yolov5s.pt file for pre-training. The model training parameters are set as shown in Table 3.

Table 3. Typeset of Papers

| model parameter | Initialization settings |
|---|---|
| Epchos | 60 |
| Batchsize | 8 |
| conf_thres | 0.25 |
| iou_thres | 0.45 |

a) Epochs

In deep learning, the number of epochs typically refers to the number of times all batches of data are processed by the model in a training cycle (epoch). The performance of the model gradually stabilizes and reaches an optimal state as the number of epochs increases, because more epochs mean the model has more opportunities to learn the data details and features, which helps the model converge. However, if the number of epochs is too high, the model may start to learn noise in the data, leading to overfitting, which results in poor performance when predicting new data. Additionally, the number of epochs affects the time and computational resources required to train the model, so a suitable balance must be found in practical applications. After tuning, it was found that if the number of epochs is too high, overfitting occurs and the training time is too long; if the number of epochs is too low, the training effect is unstable. Therefore, in this experiment, the number of epochs is set to 60, which is a good balance.

b) Batch Size

Batch size represents the amount of data processed by the network in each iteration. In deep learning, an epoch consists of multiple batch sizes. Processing more data in one iteration can improve memory utilization and training speed because more data can be processed in parallel. However, this requires higher computational hardware facilities and may lead to insufficient memory. A smaller batch size can provide better training stability and convergence, but it may affect the gradient stability during training and result in longer training time. After multiple training sessions, it was found that when the batch size is set to 8, the computer performance can be well utilized without exceeding the running memory.

c) Confidence Threshold (conf_thres)

This parameter controls the confidence threshold for identifying objects during the detection stage, determining which objects are included in the model's detection results. When the confidence threshold is high, the model will only report detection results that it is very certain about, improving precision because it is more conservative, reducing false positives. However, this may also lower the recall rate. The confidence threshold varies with different needs. After practical adjustment, it was found that when the confidence threshold is around 0.25, the precision and recall are at the best balance.

d) IOU Threshold (iou_thres)

Intersection over Union (IOU) is a metric used to measure the overlap between two bounding boxes. Setting the IOU threshold determines when two detection boxes are considered to point to the same target. When multiple bounding boxes detect the same object, the IOU threshold is used to determine which boxes to keep, filtering overlapping detection boxes. A low IOU threshold may result in multiple close detection boxes being retained, increasing false positives. A high IOU threshold can reduce this, but it may also miss

some correct detections. For gas leakage detection in this paper, the best effect is achieved with an IOU threshold of 0.45.

### 3.3. Evaluation Metrics

This model uses mean Average Precision (mAP) to evaluate the quality of the model. In addition, it also considers other evaluation metrics such as Precision, Accuracy, and Recall. The relevant calculation formulas are as follows:

$$precision = \frac{TP}{TP + FP} \tag{1}$$

$$accuracy = \frac{TP + FN}{TP + FP + FN + TN} \tag{2}$$

$$recall = \frac{TP}{TP + FN} \tag{3}$$

$$AP = \frac{\sum_{i=1}^{n} p}{n} \tag{4}$$

$$mAP = \frac{\sum_{j=1}^{c} AP}{c} \tag{5}$$

The meanings and relationships of TP, FN, FP, and TN are shown in the table below:

Table 4. Indicator Meaning

| **Confusion matrix** | | **real value** | |
|---|---|---|---|
| | | Positive | Negative |
| predicted value | Positive | TP | FP |
| | Negative | FN | TN |

TP represents true positives where the instance is true and the prediction is also true; FP represents false positives where the instance is false but the prediction is true; FN represents false negatives where the instance is true but the prediction is false; TN represents true negatives where the instance is false and the prediction is also false. P is the probability of correctly predicting the target for each image, AP is the average precision for each class, N is the number of images, C represents the total number of classes, and mAP represents the mean Average Precision across all classes.

### 3.3. Evaluation Metrics

After 60 iterations of training, the model achieved an accuracy of 98.14% in recognizing hydrogen-blended natural gas leaks, effectively enabling detection. The training variation curves are shown in Figure 5. The first and second rows of the first three images represent training loss and validation loss, respectively. Analyzing the training loss as an example, the train/box_loss plot shows the decreasing trend of bounding box regression loss during training, indicating that the model's performance in bounding box localization is gradually improving. The train/obj_loss curve shows a significant decline in object confidence loss, indicating that the model's ability to distinguish between foreground and background and determine the presence of objects is improving. Since it is a binary classification problem detecting only the presence of leaking gas, the train/cls_loss class loss curve remains stable and close to zero. The analysis of validation loss is similar to the above. The metrics/precision curve shows the proportion of actual positives among the predicted positive categories, indicating that precision improves gradually with training, and the model performs well in reducing false positives. The metrics/recall curve measures the proportion of all actual positive categories detected by the model, and the recall increases gradually, indicating that the model is missing fewer actual targets. The metrics/mAP_0.5 indicates the mean Average Precision with an IOU

threshold of 0.5, and metrics/mAP_0.5:0.95 indicates the mean Average Precision calculated over an IOU threshold range from 0.5 to 0.95. Both show a significant upward trend, indicating that the overall detection performance of the model is improving.

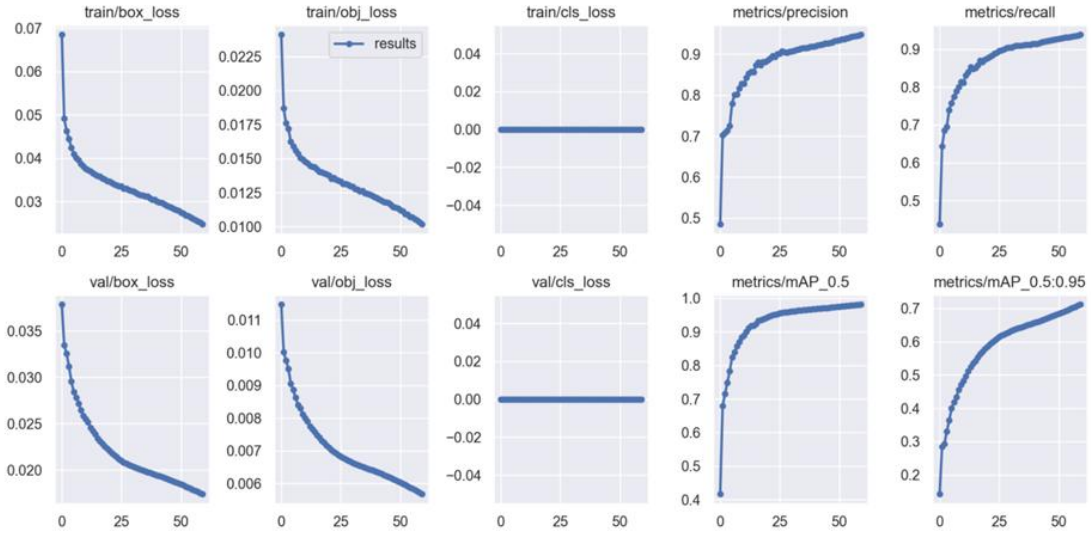


Figure 5. Training Variation Curves of the Model

After training the model using the self-constructed dataset, a new weight file, best.pt, was generated. This weight file was applied to the prediction code, making the prediction code more suitable for hydrogen-blended natural gas leakage imaging detection. The prediction results are shown in Figure 6.

In addition, the model has a preprocessing time of 0.2ms per image, an inference time of 3.4ms, and a non-maximum suppression (NMS) time of 1.7ms, which is used to eliminate duplicate bounding boxes for the final detection results. The frames per second(FPS) is 192.215, indicating that the model can process approximately 192 images per second at the specified speed. These performance metrics demonstrate that the model can handle input images of size (32, 3, 640, 640) with high processing speed and inference efficiency, enabling real-time detection and providing ample capacity to manage more complex scenarios and tasks.

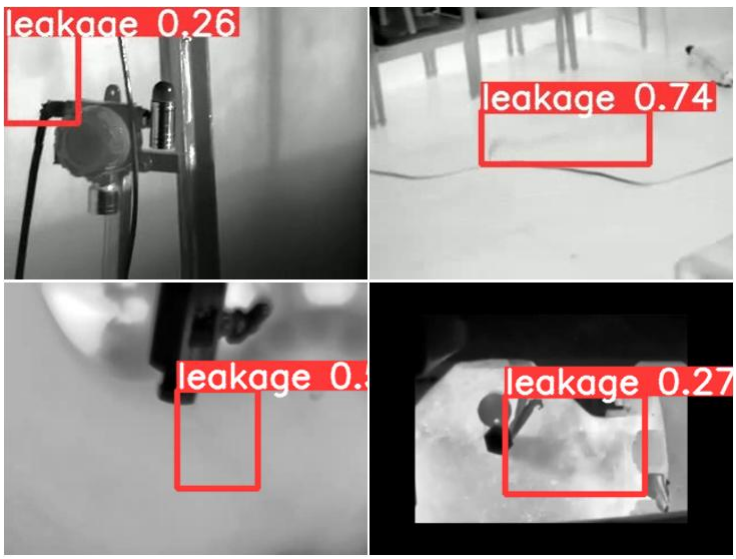


Figure 6. Model Prediction Results Display

## 4. CONCLUSION

This paper establishes a hydrogen-blended natural gas leakage simulation experimental platform, forming an infrared imaging database of hydrogen-blended natural gas leaks. It proposes an intelligent detection method for hydrogen-blended natural gas leaks based on YOLOv5. The results show that:

a) A hydrogen-blended natural gas leakage simulation experimental platform was constructed, and various scenarios and hydrogen blending ratios were collected, forming an infrared imaging dataset of hydrogen-blended natural gas leaks, laying a foundation for subsequent research.

b) After training, this method achieved a detection accuracy of 98.14% and an FPS of 192, enabling real-time detection of gas leaks in various environments. This capability provides a viable solution for the detection of hydrogen-blended natural gas leaks.

**Acknowledgements**

This paper is supported by the China Petroleum Science and Technology Innovation Fund (No. 2021DQ02-0801), and China National Petroleum Corporation-China University of Petroleum (Beijing) Strategic Cooperation Science and Technology Project: Research and Application of Key Technologies for the Integrity of Overseas Long-distance Pipelines along the Belt and Road (ZLZX2020-05).

**References**

[1] POLMAN E A, DE LAATJ C, CROWTHER M, et al. Reduction of CO2 Emissions by Adding Hydrogen to Natural Gas [R]. Apeldoorn: IEA Greenhouse R & D Programme, 2003.
[2] Zong Jiewen. Application of Optical Gas Imaging Infrared Thermography in Urban Natural Gas Leak Detection[C]//China Civil Engineering Society Gas Branch, Gas and Heating Magazine Co., Ltd. Proceedings of the 11th China Gas Operation and Safety Symposium and the 2021 Annual Conference of the Gas Branch of the China Civil Engineering Society (Volume 1), 2021: 6.
[3] Cao Jiangtao, Li Quancheng, Ban Ming, et al. A Review of Hazardous Gas Leak Detection Technology Based on Infrared Spectral Imaging[J]. Science Technology and Engineering, 2023, 23(19): 8050-8060.
[4] Wang Qi, Pan Xiatong, Xing Mingwei, et al. Research Progress on Intelligent Detection Algorithms and Quantitative Research of Passive Infrared Imaging Gas Targets[J]. Control and Decision, 2023, 38(08): 2265-2282.
[5] Weng Jing, Yuan Pan, Wang Minghe, et al. Detection Method for Leakage Gas Plume Thermal Imaging Based on Support Vector Machine[J]. Acta Optica Sinica, 2022, 42(09): 104-111.
[6] Wang J, Ji J, Ravikumar AP, Savarese S, Brandt AR. VideoGasNet: Deep Learning for Natural Gas Methane Leak Classification Using an Infrared Camera[C]. Energy, 2022, 238: 121516.
[7] Badawi D, Pan H, Cetin SC, Cetin AE. Computationally Efficient Spatio-Temporal Dynamic Texture Recognition for Volatile Organic Compound (VOC) Leakage Detection in Industrial Plants[J]. IEEE Journal of Selected Topics in Signal Processing, 2020, 14(4): 676-687.
[8] Marshall, Park JS, Song JK. FCN Based Gas Leakage Segmentation and Improvement Using Transfer Learning[C]. 2019 IEEE Student Conference on Electric Machines and Systems. Busan, 2020: 1-4.
[9] Shi J, Chang Y, Xu C, et al. Real-time leak detection using an infrared camera and Faster R-CNN technique[J]. Computers & Chemical Engineering, 2020, 135: 106780.
[10] Yang Lin, Wang Zhicheng, Gao Song. Pipeline Magnetic Flux Leakage Image Detection Algorithm Based on Multiscale SSD Network[J]. IEEE Transactions on Industrial Informatics, 2020, 16(1): 501-509.
[11] Wang J, Tchapmi LP, Ravikumar AP, McGuire M, Bell CS, Zimmerle D, Savarese S, Brandt AR. Machine Vision for Natural Gas Methane Emissions Detection Using an Infrared Camera[C]. Applied Energy, 2020, 257: 113998.
[12] Loianno V. On the Measurement of the Mutual Diffusivity of Binary Gas Mixtures with FTIR Spectroscopy[J]. Chemical Engineering Science, 2023, 270: 118546.
[13] Redmon J, Divvala S, Girshick R, Farhadi A. You Only Look Once: Unified, Real-Time Object Detection[C]. 2016 IEEE Conference on Computer Vision and Pattern Recognition (CVPR). Las Vegas, NV, USA, 2016: 779-788.